Local Normal Mode Analysis of Index-Guided AlGaAs Lasers with Mode Filter

PATRICK VANKWIKELBERGE, JEAN-PIERRE VAN DE CAPELLE, ROEL BAETS, BASTIAAN H. VERBEEK, AND JAN OPSCHOOR

Abstract—**The mode filtering properties of index-guided lasers containing a lateral mode filter section are investigated using the beam propagation method combined with a lateral local normal mode decomposition. These structures are shown to have higher kink currents than filterless devices. Furthermore, the choice of the filter length is observed to be a tradeoff between low thresholds (short filters) and suitable far fields at the filter side (long filters).**

I. Introduction

STRONG index guiding in AlGaAs semiconductor laser diodes, especially with curved active layers, has resulted in lasers with low threshold currents. The lateral mode stability of such lasers is generally poor, however, and higher order lateral modes can easily be excited, giving rise to kinks and unstable far-field patterns. Short narrow waveguides near the facets (windows) have been used successfully to filter out these higher order cavity modes [1]–[3]. In this paper, we present results of an analysis of the mode filtering properties of such narrow waveguide end regions, which prevent higher order cavity modes from reaching lasing threshold. The theoretical analysis is based on a self-consistent longitudinal laser model [4], combined with a lateral local normal mode decomposition of the calculated optical field along the device. The obtained theoretical and experimental results are compared qualitatively.

II. Device Structure

Laser structures were grown by LPE, in which the inner stripe width of 6.5 μm, defined by an internal current blocking layer, abruptly narrows down to a 3.5 μm wide stripe near the facet, the narrow section acting as the mode filter (Fig. 1). From now on, we will call the wide section of the device the laser section and the narrow section the filter section. The active layer is composed of $Al_{0.14}Ga_{0.86}As$ (wavelength $\lambda = 0.78$ μm) and surrounded by two $Al_{0.45}Ga_{0.55}As$ claddings. Owing to the LPE characteristics, the active layer in the laser section is crescent shaped, 0.11 μm thick in the center, and 0.05 μm thick towards the lateral sides, whereas the active layer is flat and 0.05 μm thick in the filter section.

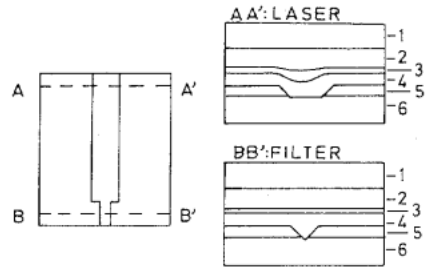

Fig. 1. Schematic diagrams of laser structure with mode filter. 1: n-GaAs top layer; 2: n-AlGaAs; 3: active layer AlGaAs; 4: p-AlGaAs; 5: n-GaAs current blocking layer; 6: p-GaAs substrate.

The main part of index guiding in the laser section is due to its crescent-shaped active layer (in fact, mainly due to the associated thickness variation), the effective index step being about $4.1\ 10^{-2}$. A smaller amount of index guiding, with an effective index step of $0.8\ 10^{-2}$, is established along the total device length through the presence of the heavily n-doped, and consequently highly absorbing, GaAs current blocking layer [5]. This is the only kind of index guiding occurring in the mode filter.

To investigate the mode filter properties, we made lasers with a filter at one side and various laser lengths (80–200 μm) and filter lengths (0–50 μm).

III. Description of the Theoretical Analysis

The theoretical analysis consists of two consecutive steps [6]. First, given the injected current at the stripe contact, the optical field and the complex effective refractive index profile are calculated iteratively in both lateral (y axis) and longitudinal (z axis) direction. A longitudinal self-consistent laser model [4] using the beam propagation method (BPM) is applied.

Next we calculate the local normal modes of the obtained lateral complex index profile for each position along the device axis so that, finally, the forward and backward propagating beams can be decomposed into these local lateral modes for all z positions.

As the examples of Section IV will show, this method of analysis gives a comprehensive insight into the device operation. We will now briefly discuss the main features of the analysis.

Manuscript received October 15, 1986. The work of P. Vankwikelberge and J. P. Van de Capelle was supported by the Belgian National Fund for Scientific Research (NFWO).

P. Vankwikelberge, J. P. Van de Capelle, and R. Baets are with the Laboratory of Electromagnetism and Acoustics, Rijksuniversiteit Gent-IMEC, B-9000 Gent, Belgium.

B. H. Verbeek and J. Opschoor are with the Philips Research Laboratories, 5600 JA Eindhoven, The Netherlands.

IEEE Log Number 8714737.

A. The Longitudinal Laser Model

Due to the longitudinally nonuniform device structure, a longitudinal laser model is used [7]. An extensive description of the applied laser model is given in [4].

The solution method of the field problem is based on the effective index method (applied to a structure with spatial variations in thickness [8]) and the BPM, taking into account both lateral and longitudinal directions. The lateral boundary conditions of the field are realized in the BPM by well-chosen (in strength and width) and equal absorbers at each end of the lateral region under consideration. These absorbers simulate the radiation condition. The longitudinal boundary conditions are determined by the Fresnel laws at the laser facets.

It is assumed that the gain and effective refractive index profile are linearly perturbed by the carrier concentration in the active layer. The effective complex refractive index is then given by the expression [4]

$$n_{\text{eff}}(y) = \left[n_{\text{eff},0}^2(y) + 2\left(\Delta n_r(y) + j \frac{g(y)}{2k_0} \right) n_a \Gamma(y) \right]^{1/2} + \Delta n_{\text{block}}(y) \tag{1}$$

in which

$n_{\text{eff},0}(y)$ = effective refractive index of unperturbed DH slab with small lateral thickness variations

n_a = unperturbed active layer refractive index (complex)

$\Gamma(y)$ = complex filling factor, depending on the active layer thickness

$g(y) = aN - b$, gain used in the wave equation

$\Delta n_r = -R(g/2k_0)$, R = index anti-guiding parameter

Δn_{block} = complex effective refractive index variation due to the blocking layer.

The functional dependence of $n_{\text{eff},0}$ and Γ on the active layer thickness W_a is assumed to be linear. Calculations have shown that in the range of interest for W_a, namely, from 0.05 up to 0.11 μm, the linearization introduces a maximum error of less than 1 percent. It should be noticed that the bend in the active layer has not been taken into account in the effective index. This bend can, however, be neglected if it is smooth and sagged over a small depth. Otherwise, an empirical refractive index distribution, representing this active layer curvature, can be included in $\Delta n_{\text{block}}(y, z)$.

The carrier concentration, necessary to define (1) completely, satisfies a nonlinear diffusion equation [9]:

$$\frac{D}{W_a(y)} \frac{d}{dy}\left(W_a(y) \frac{dN}{dy} \right) - N/\tau = -\frac{\eta J(y)}{W_a(y)\, e} + \frac{g(y)\,\Gamma(y)}{W_a(y)\, h\nu} \left| P_F(y) + P_B(y) \right| \tag{2}$$

in which N is the carrier concentration, $W_a(y)$ is the active layer thickness, D is the effective diffusion coefficient [9], N/τ is the spontaneous recombination, η is the injection efficiency, $g(y) = aN - b$ is the gain, $\Gamma(y)$ is the power-filling factor of the active layer, $h\nu$ is the photon energy, and $|P_F(y) + P_B(y)|$ is the power density per μm in the lateral direction for both traveling waves. For the injected current $J(y)$, an imposed form model is used [10], with a uniform current density at the stripe contact (the width of which is defined by the blocking layer).

Both the field problem and the diffusion equation are solved self-consistently in an iterative way until a resonance condition for the field amplitude is fulfilled. The resonance condition for the phase is not taken into account such that the longitudinal modes are not discriminated against each other, but are taken together. Multilateral cavity-mode operation at high currents does not lead to converging solutions in the iteration sheme and can therefore merely be detected. In single-mode operation, however, the optical field at each longitudinal position may well consist of more than one local normal mode in such a way that higher order modes are below threshold for the entire cavity including mode filter. For this reason, a local normal mode decomposition is applied to the field.

B. Local Normal Mode Decomposition

For each position along the laser axis, we consider the complex eigenvalue equation

$$\frac{d^2\phi}{dy^2} + \left(k^2 n_{\text{eff}}^2(y, z) - \beta^2 \right) \phi = 0 \tag{3}$$

in which $n_{\text{eff}}(y, z)$ is the complex effective refractive index profile found in Section III-A.

Equation (3) is solved by first dividing the lateral index profile into a large number of regions of constant index, in which the field can be assumed to consist of two exponential terms [10]. Next, starting with a good initial estimate of β, a Newton–Raphson iteration procedure is used to find the eigenvalues β_i of (3). The corresponding quasi-power-orthogonal eigenmodes ϕ_i are then normalized to unity power. Only the zeroth-, first-, and second-order modes will be calculated because the local higher order (>2) lateral mode content of the optical field is usually negligible in the examined situations.

The forward and backward optical beam $\phi_{F,B}$, belonging to the same cavity mode (calculated in Section III-A) can now locally be decomposed into the local modes ϕ_i:

$$\phi_{F,B}(y, z) \approx a_{0,F,B}(z)\, \phi_0(y) + a_{1,F,B}(z)\, \phi_1(y) + a_{2,F,B}(z)\, \phi_2(y) \tag{4}$$

with

$$a_{i,F,B}(z) = \int_{-\infty}^{+\infty} \phi_{F,B}(y, z)\, \phi_i(y)\, dy$$

and

$$1 = \int_{-\infty}^{+\infty} \phi_i \phi_i dy. \tag{5}$$

It turned out that the laser field does not contain the odd first-order local mode $\phi_1(y)$, and therefore we can set a_1 to zero: $a_1(z) = 0$. It should also be noticed that the forward and backward propagating beams usually have a different local normal mode content.

The phase and amplitude variations of $a_i(z)$ $(i = 0, 2)$ along the z axis, as well as the values of Re (β_i) and Im (β_i), will illustrate the influence of the mode filter on the optical field.

IV. Theoretical Examples Illustrating the Device Operation

Two types of devices are considered. First we examine devices in which the zeroth-, first-, and second-order local modes are all above cutoff along the whole structure. Next we deal with lasers having the second-order local mode below cutoff in the narrow filter waveguide. This difference among the analyzed devices is established by taking different step index-guiding profiles in the filters.

A. Filters with the Second-Order Local Mode Above Cutoff

Two devices of length 250 μm are considered, one with a 50 μm filter and one without filter (see inset of Fig. 2). The material and structural parameters are given in Table I. It should be noticed that the laser section is strongly multimodal (a 7.0 μm wide cavity with a 4.6 10^{-2} index step).

In Fig. 2, the calculated output power versus current characteristics are drawn up to the lateral multi-(cavity) mode lasing threshold. This threshold is much lower for the structure without a filter, which can be explained as follows.

If we perform a local-mode decomposition on the fundamental lateral cavity mode of the filterless laser, we find that up to its multimode threshold (further on indicated by the kink current I_{kink}), the optical field has an essentially zeroth-order (lateral) local-mode content. This means that with increasing optical power, the overlap of the gain profile with the fundamental cavity mode is deteriorating quite rapidly (due to, among other things, spatial hole burning and increasing current injection near the stripe edges). Consequently, the overlap between the gain and the first higher order cavity mode is increasing. In a strongly multimodal dielectrical cavity, this increase is quickly sufficient for that mode to reach threshold. In order to maintain single lateral mode operation up to elevated power levels, one must thus try to keep the overlap of the gain and the fundamental cavity mode as high as possible up to high excitation levels.

A way to obtain this is to introduce in the laser section a second-order lateral local-mode content beloning to the fundamental cavity mode, and this by means of a cavity-mode filter, which should be highly attenuative for higher order cavity modes as well as local modes.

The use of a 50 μm filter at one end of a 200 μm laser cavity indeed has a radical influence on the form of the field profile, as illustrated in Fig. 3 which shows the forward beam intensity of the fundamental cavity mode. The observed longitudinal interference pattern indicates the presence of a zeroth- and second-order local-(normal) mode content. A decomposition confirms this. Fig. 4 shows the amplitudes of $a_0(z)$ and $a_2(z)$. It can be seen how the second-order local mode is excited at the filter/laser interface at the cost of the zeroth-order local mode. Notice that not all of the power loss of the zeroth-order local mode is coupled into the second local mode; a small fraction is radiated sideways or coupled into higher order (>2) local modes. The distance between successive beats, as deduced from Fig. 3, is about 50 μm, which agrees well with

$$\frac{2\pi}{\text{Re}\,(\Delta\beta)} = \frac{2\pi}{\text{Re}\,(\beta_0 - \beta_2)} = 48.\ \mu\text{m}, \qquad (6)$$

β_0 and β_2 being averaged values (over the laser section).

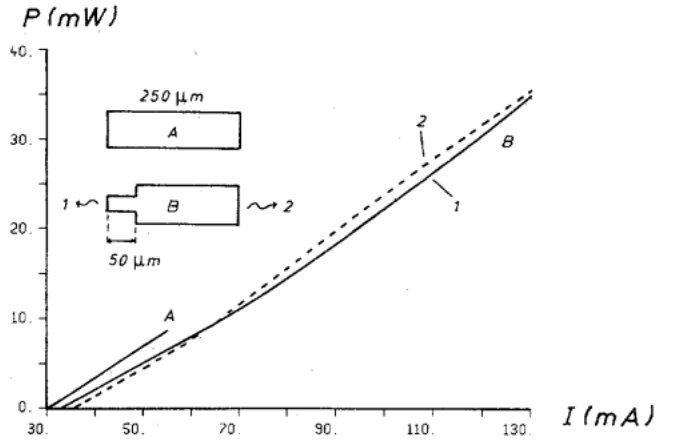

Fig. 2. Static output power versus current characteristic up to I_{kink} for A: 250 μm laser section (7. μm wide), no filter; B: 200 μm laser section (7. μm wide), 50 μm filter (4 μm wide).

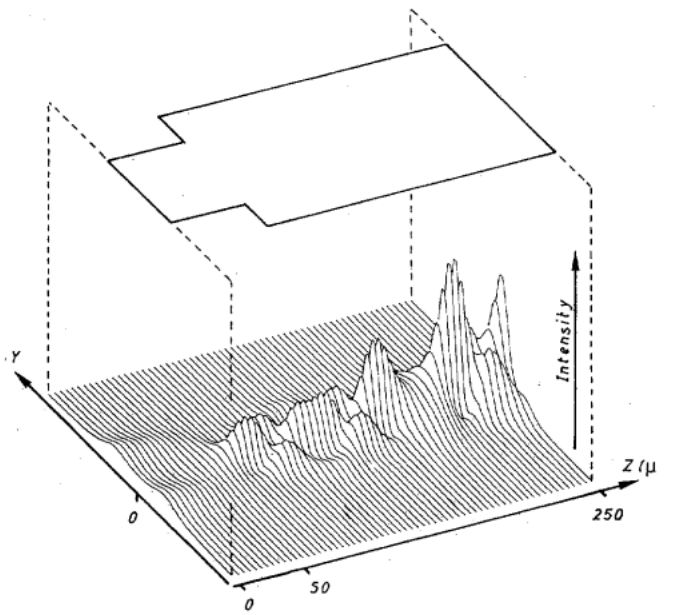

Fig. 3. Forward propagating beam of the fundamental cavity mode in window-laser structure (50 μm filter, 200 μm laser section), indicating clearly a longitudinal interference pattern.

TABLE I

Parameter	Ex. Sect. IV-A	Ex. Sect. IV-B
Stripe Width (μm)		
Laser Section s_l	4.0	3.5
Filter Section s_f	7.0	6.5
W_a (μm)		
Laser Section (Center)	0.11	0.11
Filter Section	0.05	0.05
R_1, R_2	0.32	0.32
λ (μm)	0.78	0.78
n_a	$3.61\text{-}71.6\ 10^{-6}j$	$3.61\text{-}71.6\ 10^{-6}j$
n_p	$3.37\text{-}0.21\ 10^{-3}j$	$3.37\text{-}0.21\ 10^{-3}j$
Absorption α (μm^{-1})	0.0	$9.0\ 10^{-3}$
a (μm^2)	$3.0\ 10^{-8}$	$4.35\ 10^{-8}$
b (μm^{-1})	$4.0\ 10^{-2}$	$2.0\ 10^{-2}$
Anti-Guiding Param. R	4.0	4.0
D(μm^2/ns)	3.6	3.6
τ(ns)	2.5	2.5
R_y($\Omega/\square$)	7500	7500
η	1	1
Profile of $W_a(y)$ Variation in Laser Section	$\exp(-4\sigma y^2/s_l^2)$ ($\sigma = 3.5$)	$\exp(-4\sigma y^2/s_l^2)$ ($\sigma = 6.0$)
Blocking Layer charact.		
• Step Index	$5 \cdot 10^{-3}$	$8 \cdot 10^{-3}$
• Absorber Step Outside Stripe Region (μm^{-1})	0.045	0.045
• Profile	Quasi-Step with Hamwin Filter	$\lvert y\rvert > s$: $\Delta n_{bl} = c_1$[a] $\lvert y\rvert < s - s_v$: $\Delta n_{bl} = c_2$[a] $s - s_v < \lvert y\rvert < s$: Parabolic Fit Between c_1 and c_2 ($s_v = 1.32$ μm, $s = s_l/2$, or $s_f/2$)

[a] c_1 and c_2 are complex constants deduced from the complex effective index step established by the blocking layer.

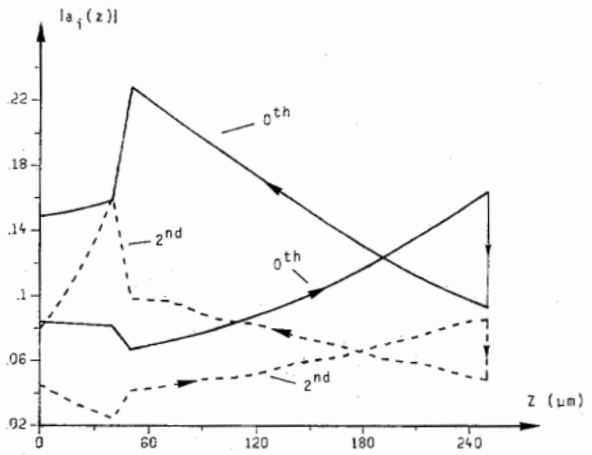

Fig. 4. Amplitude variation of the zeroth-order (solid curves) and second-order (broken curves) local-mode content of the forward and backward propagating field for $I = 45$ mA (laser structure: 50 μm filter, 200 μm laser section).

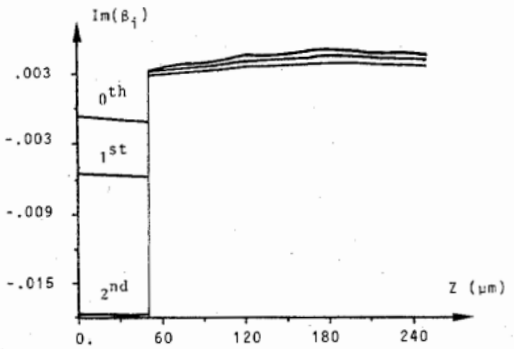

Fig. 5. Variation of the imaginary part of β_i ($i = 0, 1, 2$), indicating the local-modal gain ($=2$ Im (β_i)) variation for $I = 45$ mA.

Fig. 5 shows the Im (β_i) values; notice the positive Im (β_2) in the laser section and the negative values for all three modes in the filter section. The second-order local-mode content of the fundamental cavity mode will ameliorate the overlap of the optical field with the gain $g(y)$ in the laser section. Together with the high attenuation of that second-order content in the filter, this results in single lateral cavity-mode operation up to high injection currents.

The presence of the filter, on the other hand, also causes a slight increase of the threshold current (I_{th}) due to the attenuative character of the filter (Figs. 4 and 5). As Fig. 6 shows, the far fields (FF's) at the laser section become strongly dependent on laser output power. Moreover, calculations also showed a strong dependence of these far fields on laser lengths. However, due to the strong loss of the second-order local mode in sufficiently long filters, the far field stays Gaussian at the filter facet. Thus, by introducing filters at each laser end, Gaussian far fields

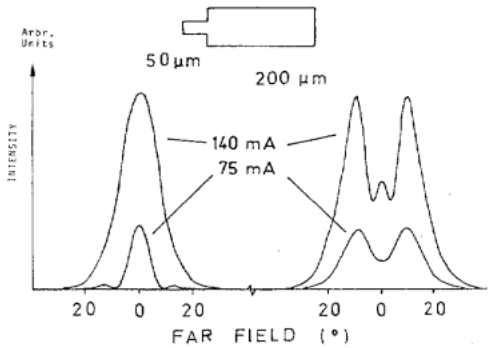

Fig. 6. Calculated far-field curves for $I/I_{th} = 1.9$ and 3.5 from both facets.

could be obtained at both facets. Notice that then there will be two exciting interfaces, demanding longer filters to obtain suitable far fields, which consequently implies higher threshold currents.

Summarized, the use of a filter causes a second-order local-mode content, with a consequently better gain/fundamental cavity-mode overlap in the wide cavity section. The filter itself, however, must sufficiently suppress that higher order content. It is the combination of both of these effects that augments I_{kink}. Therefore, lengthening the filter increases I_{kink} due to higher losses.

B. Filters with the Second-Order Local mode Below Cutoff

The device parameters are given in Table I. The laser section has a constant length of 125 μm, while several filter lengths (20, 40, and 60 μm) are considered. The step-index profile in the filter is narrowed a little as compared to the former examples in order to obtain a filter waveguide with its second-order local mode below cutoff.

Fig. 7 shows the P/I characteristics for the different structures. Again we observe a considerable increase of I_{kink} with the use of a filter. Lengthening the filter increases I_{kink} because of the substantial losses of higher order cavity modes in long filters.

For long filters, however, a power saturation effect appears at the filter facet. When the filter is too short, multicavity-mode operation is reached before any saturation can occur. The saturation phenomenon originates in the fact that the power carried by the second-order local-mode content of the backward propagating beam is radiated sideways at the interface (Fig. 8) since the mode is below cutoff in the filter. This effect becomes more explicit at high currents where the second-order local-mode power is much higher (see the mode decompostion in Fig. 8), which is mainly due to the increasing modal gain of ϕ_2 in the laser section (see Im (β_2) in Table II). Furthermore, in long filters, only a small fraction of the sideways radiated power reaches the mirror, which explains the more pronounced saturation for long filters. Fig. 9 shows the forward propagating beam in the 60 μm filter section for $I = 130$ mA. Notwithstanding the 60 μm length, there is still a small amount of sideways radiated power reflected back into the forward beam at the filter facet.

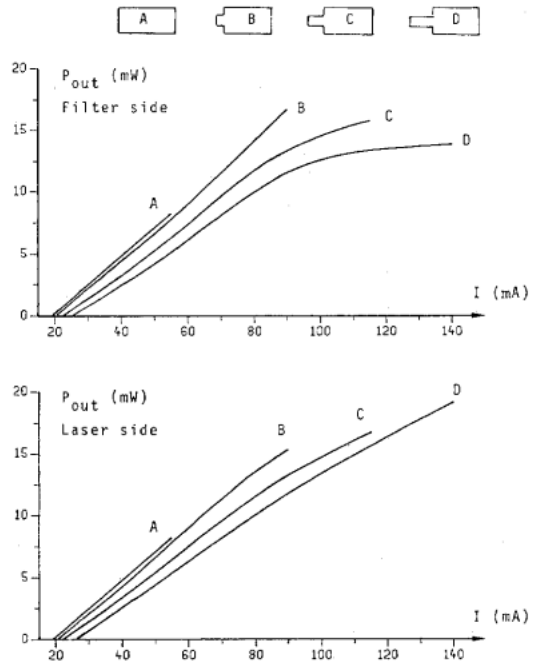

Fig. 7. Static output power (at both facets) versus current characteristic up to I_{kink} for *A*: 145 μm laser section (6.5 μm wide), no filter; *B*: 125 μm laser section (6.5 μm wide), 20 μm filter (3.5 μm wide); *C*: 125 μm laser section (6.5 μm wide), 40 μm filter (3.5 μm wide); *D*: 125 μm laser section (6.5 μm wide), 60 μm filter (3.5 μm wide).

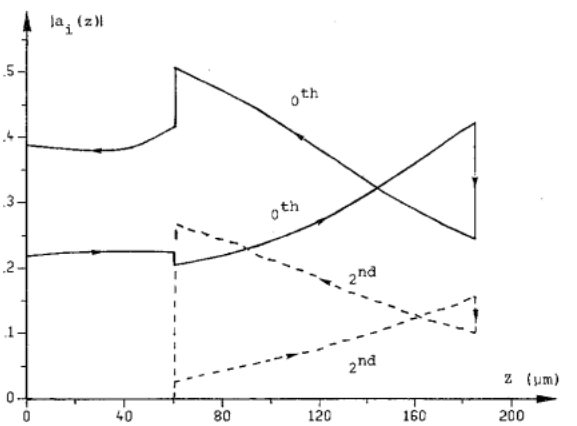

Fig. 8. Amplitude variation of the zeroth-order (solid curves) and second-order (broken curves) local-mode content of the forward and backward propagating field for $I = 130$ mA (laser structure: 60 μm filter, 125 μm laser section).

TABLE II
Im (β_i) IN THE 125 μm LASER SECTION OF A DEVICE WITH A 60 μm FILTER

Current	Im (β_0)	Im (β_1)	Im (β_2)
55 mA	$4.16\ 10^{-3}$	$3.95\ 10^{-3}$	$2.98\ 10^{-3}$
130 mA	$3.59\ 10^{-3}$	$6.78\ 10^{-3}$	$7.51\ 10^{-3}$

In spite of the strong saturation, lengthy filters have the advantage of offering the field the possibility to adapt itself to the waveguide form. Fig. 10 illustrates this by means of the axial variation of the beamwidth for structures with a 20 and 60 μm filter, respectively, at the same power level. Fig. 11 shows the associated FF's at the fil-

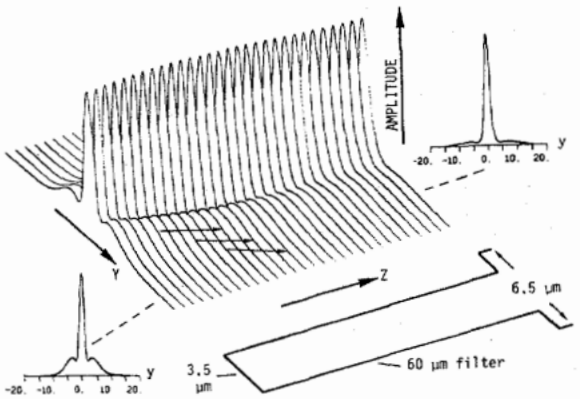

Fig. 9. Forward propagating field in the filter section, showing that some sideways radiated power is still reflected back into the forward beam at the filter facet (I = 130 mA).

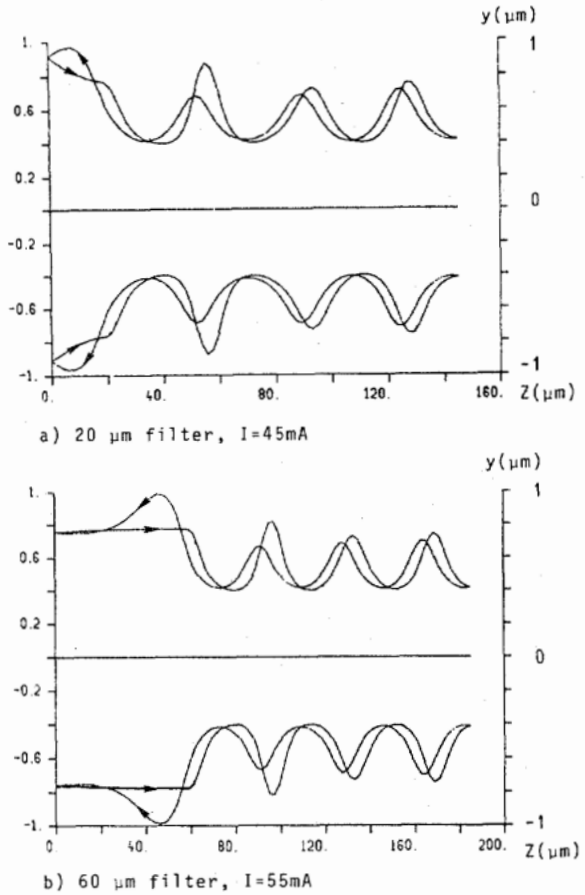

Fig. 10. Lateral position along the device of the maximal intensity and of the 3 dB points of the intensity distribution for two different structures (125 μm laser section, 20 μm, respectively, 60 μm filter) at about the same output power level (5.25 mW at the wide cavity facet).

ter facet. With the 60 μm filter, a much flatter phase front is observed (indicating low astigmatism [3]), again stressing the importance of sufficiently long filters.

V. Experimental Results

For a number of device structures, far fields (FF) from both facets were measured at various output power levels. These far fields were found to show strong dependence on

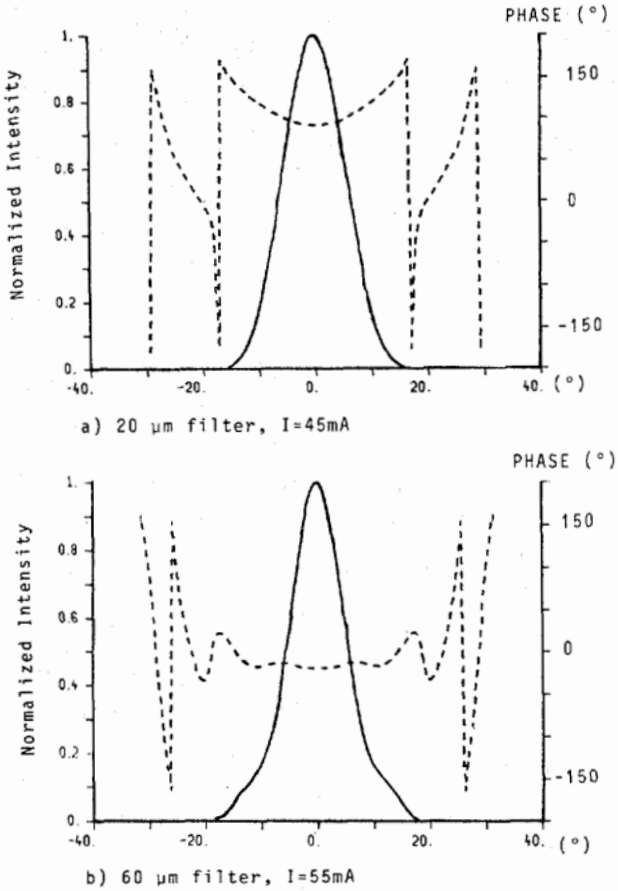

Fig. 11. Intensity and phase variation of the far field at the filter facet for two different structures (125 μm laser section, 20 μm, respectively, 60 μm filter) at about the same output power level (5.25 mW at the wide cavity facet).

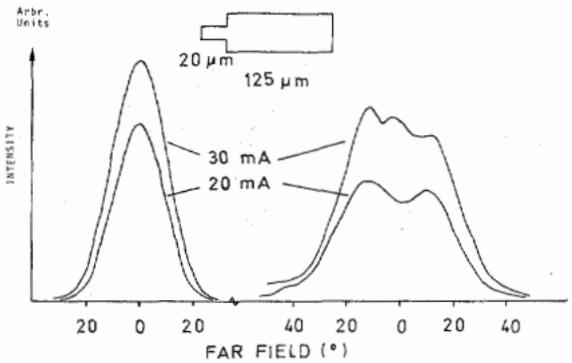

Fig. 12. Measured far-field curves for $I < I_{kink}$.

laser length and output power. Fig. 12 shows a typical example for a laser of length 125 μm and a mode filter length of 20 μm (I_{th} = 13 mA and I_{kink} = 35 mA). The FF from the wide stripe facet shows a double-lobbed peak and an additional peak near the kink current. On the other hand, the FF from the mode filter side shows a stable Gaussian peak until the higher order cavity mode is excited (not shown). The position of the kink shifts to higher currents with increasing length of the mode filter section, but I_{th} then increases.

Fig. 13 shows the calculated far fields for the example of Section IV-B with the same structure as in Fig. 12.

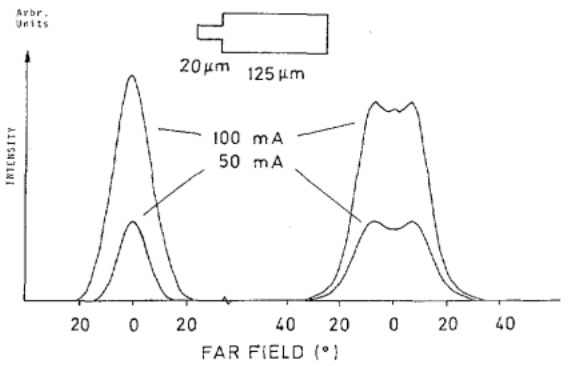

Fig. 13. Calculated far-field curves for $I < I_{kink}$.

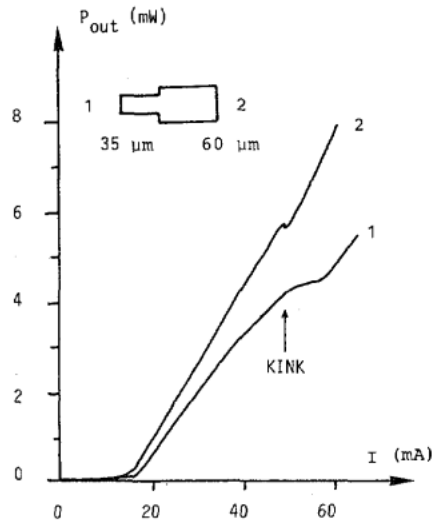

Fig. 14. Measured output power versus current characteristic for a device with a 35 μm filter (3.5 μm wide) and a 60 μm laser section (6.5 μm wide), indicating a slight saturation effect below I_{kink} at the filter facet.

Although the measured and calculated far fields differ in width and amplitude, a similar behavior is observed as a function of increasing current. However, to get a better agreement, one should take great care in the choice of the applied index profiles. Calculations have taught us that the far fields as well as I_{kink} are very sensitive to that choice (notice that the measured I_{kink} is still far below the calculated ones).

Various P/I characteristics were also measured, some showing saturation effects, others not. Fig. 14 shows a typical example for a laser of length 60 μm and a mode filter length of 35 μm (I_{th} = 14 mA and I_{kink} = 50 mA). The output power shows a slight saturation at the filter before the onset of a higher order cavity mode, while the output power curve is linear at the other facet. At both facets, Gaussian far fields are observed below the multicavity-mode lasing threshold.

VI. Conclusions

We have made strong index-guided AlGaAs lasers with one mode filter and analyzed the effect of the mode filter on the laser beam properties. A local normal mode decomposition of the optical field in this structure reveals that, at the abrupt interface between laser and filter, higher order local modes are excited, causing an increase of the lateral multicavity-mode lasing threshold.

The length and the optical waveguide properties of the filter determine the suppression of the higher order local-mode content (radiative or not) towards the filter end (important for the far fields) and also the suppression of higher order (lateral) cavity modes (due to high losses). Long filters give suitable far fields, but on the other hand, also higher threshold currents. Moreover, narrow and long filters may cause saturation at the filter facet at high currents (still below I_{kink}). This tradeoff needs to be taken into account in any design.

In conclusion, the use of mode filters allows the design of strong index-guided, wide cavity devices, having relatively low thresholds, single cavity-mode operation up to high injection levels, and suitable far fields.

Acknowledgment

The authors wish to acknowledge the skillful support of J. de Poorter in preparing the special laser chips.

References

[1] H. Kawaguchi and T. Ikegami, "Planar stripe with waist and/or notch (SWAN) injection laser," *IEEE J. Quantum Electron.*, vol. QE-16, p. 78–84, Jan. 1980.

[2] S. Yamamoto, H. Hayashi, T. Hayakawa, N. Miyauchi, S. Yano, and T. Hijikata, "High optical power CW operation in visible spectral range by window V-channeled substrate inner stripe lasers," *Appl. Phys. Lett.*, vol. 42, pp. 406–408, 1983.

[3] T. Mamine, T. Oda, and O. Yoneyama, "Analysis of astigmatism of gain guided lasers with a tapered-stripe geometry," *J. Appl. Phys.*, vol. 56, pp. 3116–3120, Dec. 1984.

[4] R. Baets, J. P. Van de Capelle, and P. E. Lagasse, "Longitudinal analysis of semiconductor lasers with low reflectivity facets," *IEEE J. Quantum Electron.*, vol. QE-21, pp. 693–699, June 1985.

[5] S. R. Chinn and R. J. Spiers, "Calculation of separated multicladlayer stripe geometry laser modes," *IEEE J. Quantum Electron.*, vol. QE-18, pp. 984–991, June 1982.

[6] B. H. Verbeek, J. Opschoor, P. Vankwikelberge, J. P. Van de Capelle and R. Baets, "Analysis of index-guided AlGaAs lasers with mode filter," *Electron. Lett.*, vol. 22, pp. 1022–1023, Sept. 1986.

[7] G. P. Agrawal, "Fast-Fourier-transformed based beam propagation model for stripe geometry semi-conductor lasers: Inclusion of axial effects," *J. Appl. Phys.*, vol 56, pp. 3100–3109, Dec. 1984.

[8] W. Streifer, R. D. Burnham, and D. R. Scifres, "Analysis of diode lasers with lateral spatial variations in thickness," *Appl. Phys. Lett.*, vol. 37, pp. 121–123, July 1980.

[9] W. B. Joyce, "Carrier transport in double heterostructure active layers," *J. Appl. Phys.*, vol. 53, pp. 7235–7239, 1982.

[10] J. Buus, "Models for the static and dynamic behavior of stripe geometry lasers," *IEEE J. Quantum Electron.*, vol. QE-19, pp. 953–959, June 1983.

Patrick Vankwikelberge was born in Gent, Belgium, on May 20, 1962. He received the degree in electrical engineering from the University of Gent in 1985.

He is presently working toward the Ph.D. degree in electrical engineering at the University of Gent. His main research interests include the dynamic properties of semiconductor lasers and quantum well lasers.

Jean-Pierre Van de Capelle was born in Gent, Belgium, on March 12, 1961. He received the degree in electrical engineering (summa cum laude) from the University of Gent in 1984.

He is currently working toward the Ph.D. degree at the University of Gent. His interests include the modeling and fabrication of semiconductor lasers. He is the author or coauthor of approximately 10 publications in international journals and conference proceedings.

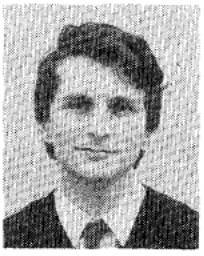

Roel Baets received the degree in electrical engineering from the University of Gent, Gent, Belgium, in 1980. He received the M.Sc. degree in electrical engineering from Stanford University, Stanford, CA, and the Ph.D. degree from the University of Gent in 1981 and 1984, respectively.

Since 1984 he has been employed by the Interuniversity Microelectronics Center (IMEC) and is responsible for the optoelectronics activities in the III–V group at the University of Gent. His interests include epitaxial growth of III–V compounds and optoelectronic devices, especially laser diodes.

Bastiaan H. Verbeek received the M.Sc. and Ph.D. (cum laude) degrees from the State University of Leiden, Leiden, The Netherlands, in 1975 and 1979, respectively.

In 1979 he joined the Metals Research Group at Philips Research Laboratories, Eindhoven, The Netherlands, where he studied the electronic structure of metallic compounds with synchroton radiation. In 1983 he joined the Semiconductor Laser Group, where he is engaged in optical properties and feedback effects of AlGaAs semiconductor lasers.

Jan Opschoor was born in Krimpen aan den IJssel, The Netherlands, on January 6, 1957. He received the M.S. degree (cum laude) in chemical engineering from the Delft University of Technology, Delft, The Netherlands, in 1981.

In 1982 he joined Philips Research Laboratories, Eindhoven, The Netherlands, where he is working on GaAlAs/GaAs semiconductor lasers. His current interests are in index-guided phased coupled arrays.